Mineralogical Magazine, December 2011, Vol. 75(6), pp. 2833–2846

Essential features of the polytypic charoite-96 structure compared to charoite-90

Dedicated to the memory of Professor Friedrich Liebau (deceased March 11, 2011)

I. V. ROZHDESTVENSKAYA[1,2,*], E. MUGNAIOLI[3], M. CZANK[2], W. DEPMEIER[2], U. KOLB[3] AND S. MERLINO[4]

[1] Department of Crystallography, Geological Faculty, Saint Petersburg State University, University emb. 7/9, St Petersburg 199034, Russia
[2] Department of Crystallography, Institute of Geosciences, Christian-Albrechts-University, Olshausenstrasse 40, D-24098 Kiel, Germany
[3] Institute of Physical Chemistry, Johannes Gutenberg-University, Welderweg 11, D-55099 Mainz, Germany
[4] Dipartimento di Scienze della Terra, University of Pisa, I-56126 Pisa, Italy

[*Received 2 June 2011; Accepted 8 September 2011*]

ABSTRACT

Charoite, ideally $(K,Sr,Ba,Mn)_{15-16}(Ca,Na)_{32}[(Si_{70}(O,OH)_{180})](OH,F)_4 \cdot nH_2O$, is a rock-forming mineral from the Murun massif in Yakutia, Sakha Republic, Siberia, Russia, where it occurs in a unique alkaline intrusion. Charoite occurs as four different polytypes, which are commonly intergrown in nanocrystalline fibres. We report the structure of charoite-96 (a = 32.11(6), b = 19.77(4), c = 7.23(1) Å, β = 95.85(9)º, V = 4565(24) Å^3, space group $P2_1/m$), which was solved *ab initio* by direct methods on the basis of 2676 unique electron diffraction reflections collected by automated diffraction tomography and refined to R_1/wR_2 = 0.34/0.37. The structure of charoite-96 is related to that of the charoite-90, which was also solved recently. Both structures are composed of three different types of *dreier* silicate chains running along [001] and separated by ribbons of edge-sharing Ca- and Na-centred octahedra. In the structure of charoite-96, adjacent blocks formed by three different silicate chains and stacked along the x axis, are shifted by a translation of ½ c. The shifts involve a hybrid *dreier* quadruple chain, $[Si_{17}O_{43}]^{18-}$ and a double *dreier* chain, $[Si_6O_{17}]^{10-}$. In charoite-90 adjacent blocks are stacked without shifts.

KEYWORDS: charoite polytypes, electron crystallography, crystal structure analysis, electron diffraction, electron diffraction tomography.

Introduction

POLYTYPISM is a relatively common phenomenon in silicate minerals (Ferraris *et al*., 2004). In chain silicates, polytypism is most commonly connected with stacking faults or shifts of crystal structure blocks. One of the best known examples of this type of polytypism is in the *dreier* chain silicate wollastonite (nomenclature according to Liebau, 1985; see also Jefferson and Bown, 1973; Wenk *et al*., 1976). In wollastonite, $CaSiO_3$, the octahedral bands and tetrahedral silicate chains run along the z axis. The c lattice parameter is ~7.3 Å; it spans two octahedral edges and one repeat period of the tetrahedral silicate chain, respectively. The spatial relationships between octahedral fragments and tetrahedral silicate chains permit the tetrahedral chain to be connected to the octahedral fragment at two distinct positions, which are ~3.65 Å apart along the chain axis.

Recently, we described the structure of charoite-90, which consists of three different *dreier* silicate chains parallel to the z axis (Rozhdestvenskaya *et al*., 2010). Apical oxygen atoms bond the chains to bands of parallel-

* E-mail: ivrozhdestvenska@mail.ru
DOI: 10.1180/minmag.2011.075.6.2833

running Ca- and Na-bearing octahedra of variable width in two distinct ways. In common with wollastonite and various hydrated calcium silicates (e.g. xonotlite and tobermorite) this produces an OD (Order–Disorder) character. The OD character (Dornberger-Schiff, 1956, 1964, 1966; Ferraris *et al.*, 2004) of charoite was described by Rozhedestvenskaya *et al.* (2010). The main features are illustrated in Fig. 1. The OD layers, with *P*(2)*mm* symmetry, succeed each other along *a*; adjacent layers are related by the operations (σ-operations in OD terminology) $2_{1/2}$ or $2_{-1/2}$, parallel to *c*. An infinite number of polytypes or disordered sequences are possible, but there are only two main polytypic MDO (maximum degree of order) structures, characterized by similar sequences of layers: MDO1 is produced by the regular alternation of the operations $2_{1/2}$ and $2_{-1/2}$ and MDO2 is produced by the constant application of the operation $2_{-1/2}$ (the constant application of the operation $2_{1/2}$ gives rise to a structure that is twin-related to the previous one).

Selected area electron diffraction (SAED) patterns of different fibres along [010] have revealed the presence of four structural arrangements (Fig. 2). The two simplest polytypic MDO structures have clearly related cell parameters and monoclinic symmetry (Fig. 2*a*,*b*). These are described as 'charoite-96' (MDO2) and 'charoite-90' (MDO1), on the basis of their monoclinic angles, β = 96º and β = 90º respectively. Some SAED patterns indicate a doubling of the *a* parameter in all *h*0*l* diffraction lines, which suggests a third possible charoite polytype ('charoite-2a', Fig. 2*c*), which is probably produced by the $2_{1/2}$, $2_{1/2}$, $2_{-1/2}$, $2_{-1/2}$... sequence of σ-operations. The presence of diffuse streaks along *h*0*l* (*l* = 2*n*+1) lines and of disordered intergrown fine lamellae in high resolution

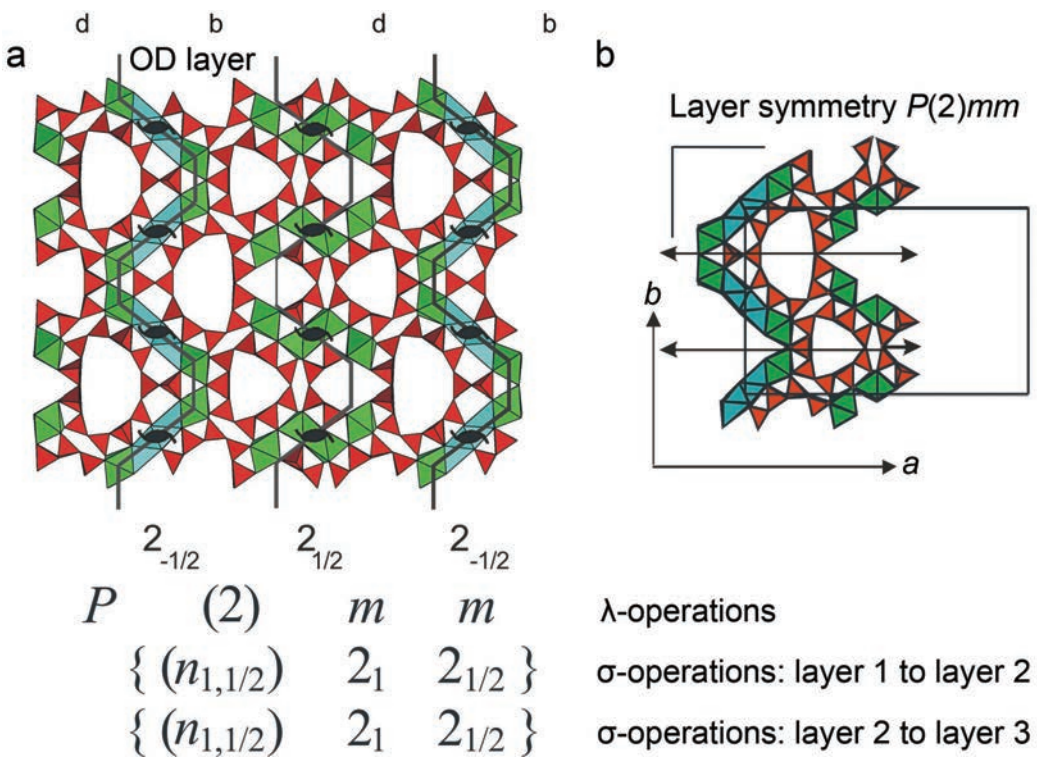

FIG. 1. The OD character of charoite. (*a*) The structural arrangement in charoite-90 represented as seen down *c*, with *a* horizontal. The layers are polar with respect to the stacking direction and regularly invert their polarity, as indicated by the letters d, b, d, b... The stacking of the OD layers shown in (*b*) is related by $2_{1/2}$ or $2_{-1/2}$ σ-operations.

transmission electron microscopy (TEM) images suggests a disordered sequence of OD layers ('charoite-d', Fig. 2*d*) (Rozhdestvenskaya *et al*., 2010). Using modified Gard notation (Bailey, 1977) and the nomenclature for polytypes agreed by the International Union of Crystallography (IUCr) and the International Mineralogical Association (IMA), these polytypes can be described as: charoite-90, ψOabc; charoite-96, Mabc; charoite-2a, ψO2abc and charoite-d, Ma_dbc.

In this paper we report an investigation of the charoite-96 polytype by automated electron diffraction tomography (ADT) and precession electron diffraction (PED), which allowed its structure to be determined *ab initio*.

Experimental

The rock sample used in the investigations consists of charoite fibres with minor quartz, apophyllite, pectolite, acmite and K-feldspar (Rozhdestvenskaya *et al*., 2010). For TEM and ADT analysis the sample was powdered and deposited on a carbon-coated copper grid. Identification of charoite crystallites is straightforward due to their high aspect ratio and large cell parameters, which are easily recognized in the diffraction patterns. The width of the charoite fibres ranges from ~100 nm to a few μm; the length normally exceeds 10 μm. Despite an extensive search, a fibre consisting of a single coherent charoite-96 domain was not found. Therefore the tip of a fibre consisting of two domains, one of charoite-96 and one of charoite-90, was chosen for electron diffraction intensity collection (Fig. 3). The boundary between the two domains runs parallel to (100) and is therefore parallel to the long axis of the fibre; it delimits two elongated coherent crystallites. The *z* and *y* axes of the charoite-96 domain are parallel to the corresponding axes of the charoite-90 domain. The charoite-96 domain is ~400 nm wide when the fibre is set at 0º tilt, but its effective width is reduced and the domains partially overlap at higher tilt angles.

The ADT measurements were carried out using a FEI TECNAI F30 S-TWIN transmission electron microscope operating at 300 kV at the Institute of Physical Chemistry, Johannes

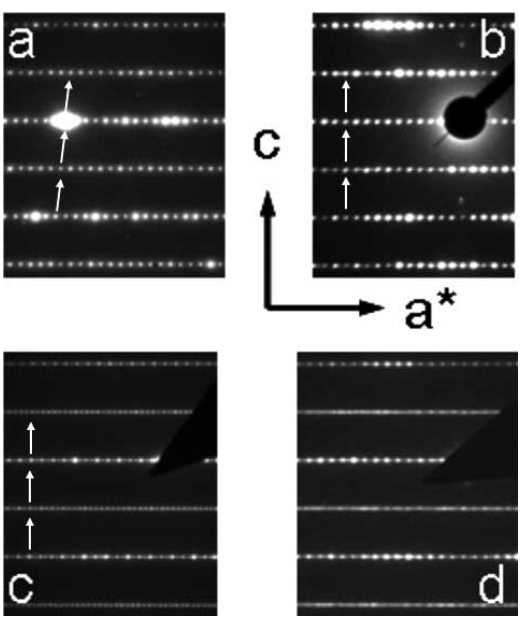

FIG. 2. The [010] SAED patterns of the polytypes: (*a*) charoite-96; (*b*) charoite-90; (*c*) charoite-2a and (*d*) charoite-d (from Rozhdestvenskaya *et al*., 2010).

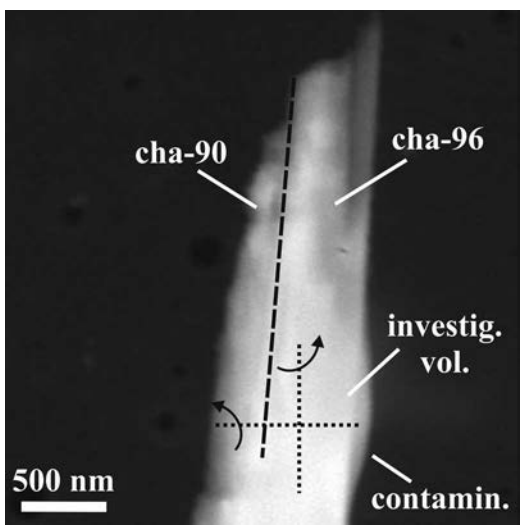

FIG. 3. The charoite fibre selected for ADT acquisition. The fibres contains two domains, charoite-90 (cha-90) and charoite-96 (cha-96), that partially overlapped during tilting. The black dashed line marks the border between the two domains. The volume from which ADT data were collected is indicated, as is the overgrowth of contamination that accumulated during the acquisition. The tracks of the two orthogonal tilt axes of the ADT acquisitions are marked as black dotted lines.

Gutenberg-University, Mainz, following reconnaissance studies using a Philips EM400T instrument at the Department of Crystallography, Institute of Geosciences, Christian-Albrechts-University, Kiel. Electron diffraction patterns from nano-scale areas were acquired using a CCD camera (14-bit GATAN 794MSC). Scanning transmission electron microscopy (STEM) images were acquired using a FISCHIONE high angular annular dark field (HAADF) detector.

For structure analysis, 3D electron diffraction data were acquired with a FISCHIONE tomography holder, using the automated module described in Kolb *et al.* (2007). A 10 μm condenser aperture and relatively low energy conditions (gun lens at step 8; spot size at step 6) were used to produce a quasi-parallel electron beam 70 nm in diameter, which reduced damage to the sample. Precession electron diffraction (PED) was coupled with ADT to improve the reflection intensity quality (Vincent and Midgley 1994; Mugnaioli *et al*., 2009). In PED the electron beam is tilted at a small angle (the precession angle) and rotated around a vertical axis at high speed. The varying tilt angle of the Ewald sphere reduces both the dynamic scattering and excitation error and the diffraction pattern appears steady due to the high speed of rotation. The PED analyses were performed using a NanoMEGAS SpinningStar unit. The precession angle was set at 1.2º.

Self-developed software packages and *ADT3D* software (Kolb *et al.*, 2008; Schömer *et al.*, 2009) were used for data processing including 3D reciprocal space reconstruction and inspection, cell parameter determination, and intensity integration. The estimated standard deviations for intensities were set to $(\text{Intensity})^{-1/2}$ to ensure consistent structure analyses using *SIR2008* (Burla *et al.*, 2007) and *SHELXL97* (Sheldrick, 2008).

Ab initio structure solution and difference Fourier maps

Two precessed ADT tilt series with orthogonal tilt axes were taken from the charoite-96 domain, as described in Mugnaioli *et al.* (2009) and Rozhdestvenskaya *et al.* (2010). The tilt step was 1º and the tilt range was 120º for the first acquisition and 110º for the second one. Despite the care taken during ADT acquisition, diffraction spots from the charoite-90 domain were sampled in some of the diffraction patterns. The reconstructed 3D reciprocal space for the first tilt series is shown in Fig. 4*a*–*d*. An electron diffraction intensity data set was obtained by merging the two tilt series. No merging factor was applied. Unit-cell parameters, data acquisition information and refinement parameters are listed in Table 1.

The $R_{sym}(F)$ of the intensity data set was 22%. This value is relatively high due to the partial sampling of the charoite-90 domain during ADT acquisition. Charoite-90 reflections overlap with charoite-96 reflections if $l = 2n$, and they are relatively close if $l = 2n+1$ (Fig. 4*c*). As the strongest reflections are in the *hkl* planes with $l = 2n$, the accuracy of the structure determination is limited by the experimental error introduced by reflections from charoite-90. The partial overlapping of the two data sets at higher tilt angles means that reflections from charoite-90 were collected accidentally and in an unknown ratio to those of charoite-96.

TABLE 1. Crystallographic data and experimental and refinement parameters for charoite structure.

a (Å)	32.11(6)
b (Å)	19.77(4)
c (Å)	7.23(1)
β (º)	95.85(9)
V (Å^3)	4566(24)
Space group	$P2_1/m$
F_{000}	3529
Crystal size (μm)	$10 \times 0.4 \times 0.1$
λ (Å)	0.0197
$2\theta_{max}$ (º)	1.01
$(\sin\theta/\lambda)_{max}$	0.447
$(h,k,l)_{max}$	28, 17, 6
Total reflections	10,271
Independent reflections	3353
Resolution (Å)	1.15
R_{sym} (by SIR)	0.22
R_σ	0.048
Completeness (%)	97
R_{eqv}	0.345
Unique with $\lvert F_o\rvert > 4.0\sigma_F$	2676
R_1	0.339
wR_2	0.375
GOF	0.93
Ws	$1/[\sigma^2_{F^2} + (0.25\ F^2_{obs})]$

Note: $R_1 = \Sigma\lvert\lvert F_o\rvert - \lvert F_c\rvert\rvert / \Sigma\lvert F_o\rvert$;
$wR_2 = \{\Sigma[w(F_o^2 - F_c^2)^2] / \Sigma[w(F_o^2)]\}^{1/2}$;
$GOF = \{\Sigma[w(F_o^2 - F_c^2)]/(n-p)\}^{1/2}$, where n is the number of reflections and p is the number of refined parameters.

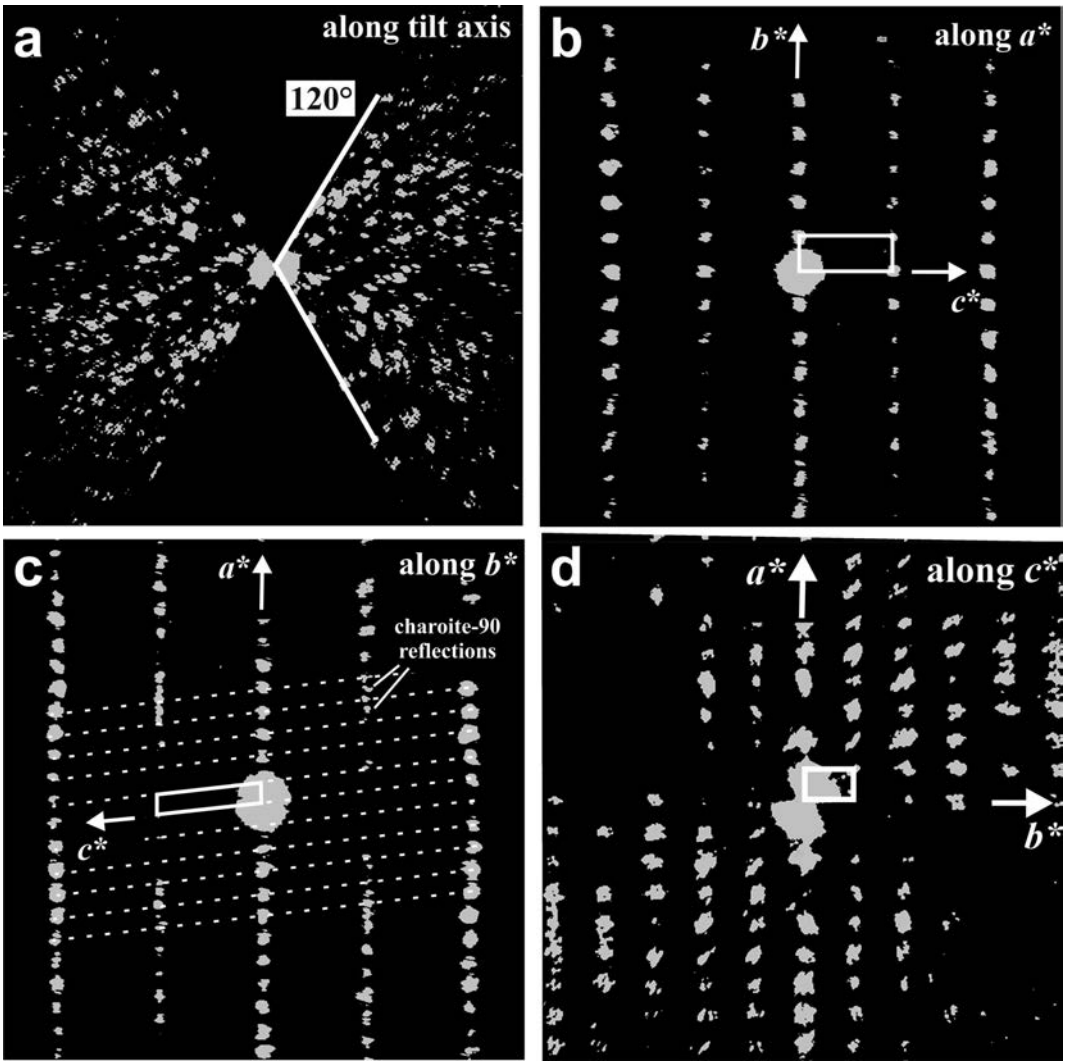

FIG. 4. Three-dimensional reciprocal space reconstructed from the first ADT tilt acquisition: (*a*) view along the tilt axis showing the collected wedge of 120º; (*b*) projection along *a**; (*c*) projection along *b**, reflections from charoite-90 are indicated; (*d*) projection along *c**. The smearing of reflections is due to PED technique. The unit-cell and main-reciprocal directions are indicated in white. It should be noted that these are not two-dimensional diffraction zone patterns, but projections of three-dimensional reciprocal space. Therefore, the extinctions due to screw axes are not visible.

The structure solution was performed in space group $P2_1/m$ as determined by Rozhdestvenskaya *et al.* (2009). The structure was solved *ab initio* by direct methods implemented in SIR2008 (Burla *et al.*, 2007) using a fully kinematical approach. Intensities were assumed to be proportional to F^2_{hkl}. The best solution obtained was with $R(F) = 0.35$ and an overall atomic displacement parameter U_{overall} of 0.024 Å^2. A total of 8 Ca/Na, 20 Si and 46 O positions were correctly identified. The positions of the 5 missing oxygen atoms in the framework and the channel content (7 K/Sr ions and 1 H_2O molecule) were determined using difference Fourier maps calculated using

SHELXL97 (Sheldrick, 2008) and *CSD* (Akselrud *et al.*, 1989).

Least-squares refinement

Least-squares refinements were performed with *SHELXL97* and *CSD*, using 2676 reflections with $F(hkl) > 4\sigma_F$, and leading to $R_1(F)/wR_2(F^2)$ = 0.34/0.37. This relatively high residual almost certainly results from the overlap of diffraction intensities from the charoite-90 domain with about 50% of the charoite-96 reflections. The intensities of equivalent reflections varied significantly (R_{eqv} = 0.34). The number of independent atom positions is 87 and the number of free variables 335. A first refinement without geometrical restraints and with full occupancies converged to a residual $R_1(F)$ = 0.27. In this model the Ca/Na−O and Si−O distances average 2.37(13) and 1.64(17) Å, respectively. These errors are similar to those reported for other structure solutions by ADT electron diffraction, despite the overlapping reflections (Mugnaioli *et al*. 2009, 2011).

As an unrestrained refinement produced unrealistic interatomic distances, restraints on the mean

TABLE 2. Atom coordinates, isotropic displacement parameters (Å^2) and occupancies of the charoite-96 structure.

Site	*N**	*x*	*y*	*z*	U_{iso}/U_{eq}** × 100	Occupancy***
Na(1)	4	0.9601(8)	0.0686(14)	0.364(4)	3.1(9)	0.94(6) Na
Na(2)	4	0.9649(10)	0.0708(16)	0.845(4)	2.5(9)	0.89(6) Na
Ca(1)	4	0.8773(6)	0.14569)	0.569(9)	5.2(6)	
Ca(2)	4	0.8731(5)	0.1464(8)	0.065(2)	3.2(5)	
Ca(3)	4	0.5411(5)	0.0442(8)	0.896(2)	4.8(6)	
Ca(4)	4	0.5413(5)	0.0434(9)	0.395(2)	2.5(4)	
Ca(5)	4	0.3514(5)	0.0663(8)	0.050(2)	4.3(4)	
Ca(6)	4	0.3481(4)	0.0697(7)	0.542(2)	2.0(5)	
K(1)	2	0.4834(9)	¼	0.605(4)	4.5(5)	
K(2)	2	0.5963(12)	¼	0.185(5)	9.2(9)	
K(3)	4	0.7364(7)	0.1201(11)	0.248(3)	3.8(4)	0.85(3) K
K(4)	2	0.3584(13)	¼	0.306(6)	8.3(8)	
K(5)	2	0.6971(14)	¼	0.761(6)	5.1(6)	0.92(5) K
K(6)	4	0.2002(14)	0.051(2)	0.189(5)	5.2(9)	0.48(4) K
Sr	2	0.3608(10)	¼	0.849(5)	5.6(13)	0.69(3) Sr
Si(1)	4	0.4953(6)	0.1717(10)	0.134(3)	2.6(7)	
Si(2)	4	0.4392(9)	0.0965(14)	0.383(4)	6.8(9)	
Si(3)	4	0.4413(8)	0.1030(12)	0.815(4)	4.5(8)	
Si(4)	4	0.5866(7)	0.1741(12)	0.662(3)	3.0(7)	
Si(5)	4	0.6409(8)	0.1029(11)	0.413(3)	4.5(8)	
Si(6)	4	0.6408(6)	0.1039(10)	0.987(3)	4.0(7)	
Si(7)	4	0.6966(8)	0.0578(11)	0.712(3)	3.5(7)	
Si(8)	4	0.7849(7)	0.1440(11)	0.765(3)	4.7(8)	
Si(9)	2	0.7910(10)	¼	0.050(4)	1.8(8)	
Si(10)	2	0.7941(9)	¼	0.482(3)	3.0(9)	
Si(11)	4	0.2667(7)	0.1775(12)	0.481(3)	5.2(8)	
Si(12)	4	0.2638(6)	0.1794(9)	0.041(3)	2.6(6)	
Si(13)	4	0.2558(7)	0.0671(12)	0.736(3)	4.9(8)	
Si(14)	4	0.8271(9)	0.0144(13)	0.299(4)	7.5(9)	
Si(15)	4	0.1048(7)	0.0245(14)	0.945(3)	2.6(6)	
Si(16)	4	0.1046(9)	0.0245(14)	0.392(4)	7.0(9)	
Si(17)	4	0.0561(8)	0.1051(11)	0.660(3)	5.9(9)	
Si(18)	2	0.0209(8)	¼	0.652(4)	1.6(8)	
Si(19)	2	0.9429(8)	¼	0.885(4)	3.5(9)	
Si(20)	2	0.9448(10)	¼	0.318(5)	7.3(9)	
O(1)	2	0.511(2)	¼	0.159(9)	8.0(2)	
O(2)	4	0.466(1)	0.157(2)	0.946(5)	3.5(7)	
O(3)	4	0.464(1)	0.166(2)	0.302(5)	4.1(8)	

TABLE 2 (*contd.*).

Site	*N**	*x*	*y*	*z*	U_{iso}/U_{eq}** × 100	Occupancy***
O(4)	4	0.532(1)	0.120(2)	0.137(5)	6.0(9)	
O(5)	4	0.438(2)	0.125(3)	0.592(6)	7.8(11)	
O(6)	4	0.3908(9)	0.100(2)	0.308(5)	8.4(12)	
O(7)	4	0.472(1)	0.035(2)	0.395(6)	5.9(9)	
O(8)	4	0.393(1)	0.112(3)	0.803(7)	4.9(8)	
O(9)	4	0.466(1)	0.032(2)	0.870(5)	3.9(7)	
O(10)	2	0.571(3)	¼	0.724(13)	12.0(3)	
O(11)	4	0.6151(8)	0.163(1)	0.487(4)	3.8(7)	
O(12)	4	0.609(1)	0.163(2)	0.885(5)	3.4(7)	
O(13)	4	0.550(1)	0.119(2)	0.632(5)	4.2(7)	
O(14)	4	0.6845(7)	0.103(1)	0.538(3)	1.9(5)	
O(15)	4	0.649(1)	0.132(2)	0.205(4)	4.1(7)	
O(16)	4	0.616(1)	0.033(2)	0.386(6)	6.4(9)	
O(17)	4	0.685(1)	0.091(3)	0.894(6)	6.2(9)	
O(18)	4	0.613(1)	0.040(2)	0.948(7)	6.4(9)	
O(19)	4	0.7473(8)	0.081(1)	0.736(4)	1.7(6)	
O(20)	4	0.306(1)	0.025(2)	0.272(5)	6.6(10)	
O(21)	4	0.776(1)	0.183(2)	0.565(5)	3.7(7)	
O(22)	4	0.7713(9)	0.184(1)	0.939(4)	3.6(7)	
O(23)	4	0.834(1)	0.116(2)	0.777(6)	8.8(12)	
O(24)	2	0.777(2)	¼	0.264(5)	8.0(2)	
O(25)	2	0.841(2)	¼	0.073(13)	6.3(13)	
O(26)	2	0.844(1)	¼	0.537(6)	2.0(8)	
O(27)	2	0.249(1)	¼	0.516(5)	2.4(9)	
O(28)	4	0.242(2)	0.113(2)	0.553(6)	5.6(9)	
O(29)	4	0.249(2)	0.171(3)	0.248(5)	7.5(11)	
O(30)	4	0.313(1)	0.176(2)	0.518(6)	4.5(8)	
O(31)	2	0.246(2)	¼	0.941(8)	8.1(16)	
O(32)	4	0.251(2)	0.125(3)	0.890(9)	9.3(13)	
O(33)	4	0.313(1)	0.187(2)	0.030(6)	3.5(7)	
O(34)	4	0.221(1)	0.009(2)	0.745(7)	4.6(8)	
O(35)	4	0.300(1)	0.031(2)	0.765(5)	9.5(13)	
O(36)	4	0.150(1)	0.032(2)	0.851(6)	5.8(9)	
O(37)	4	0.147(1)	0.012(2)	0.516(4)	3.4(7)	
O(38)	4	0.836(1)	0.098(2)	0.298(6)	6.2(9)	
O(39)	4	0.082(3)	0.086(3)	0.843(9)	7.7(11)	
O(40)	4	0.111(1)	0.043(2)	0.172(4)	8.2(12)	
O(41)	4	0.920(1)	0.044(2)	0.079(6)	6.0(9)	
O(42)	4	0.915(1)	0.045(2)	0.607(5)	4.9(8)	
O(43)	4	0.081(1)	0.089(2)	0.476(6)	3.9(7)	
O(44)	4	0.0519(9)	0.186(1)	0.628(4)	3.3(7)	
O(45)	4	0.014(2)	0.058(3)	0.634(9)	6.4(10)	
O(46)	2	0.987(1)	¼	0.795(6)	3.6(10)	
O(47)	2	0.980(2)	¼	0.492(7)	8.0(16)	
O(48)	2	0.958(3)	¼	0.107(6)	13.0(3)	
O(49)	4	0.925(1)	0.176(1)	0.841(4)	6.1(9)	
O(50)	4	0.920(1)	0.176(1)	0.334(5)	8.8(12)	
OH	4	0.007(2)	0.047(4)	0.143(9)	9.2(13)	0.5 OH +0.5 F
H_2O	2	0.697(2)	¼	0.261(8)	18.0(10)	0.41(3) O

* *N* is the multiplicity.
** $U_{eq} = 1/3[U_{11}a^{*2}a^2 + ... + 2U_{23}b^*c^*bc\cos(\alpha)]$.
*** Only the occupancy of mixed sites is shown. All other sites are fully occupied by the element.

Ca/Na−O (2.40 Å) and Si−O (1.61 Å) distances were imposed and the occupancies of the two Na sites and six K and Sr sites were refined. The structure refinement (see Table 2 for details) converged to a residual of $R_1(F) = 0.34$. The weighted residual $wR_2(F^2)$ calculated using the standard weighting scheme for X-ray diffraction data is 0.37. Isotropic atom displacement parameters all fall in a reasonable range. Selected interatomic distances are reported in Table 3.

The model reveals the relevant topological and geometrical features of the structure. Despite the high residual, the structure of charoite-96 is considered to be correct as the atom positions are clearly identified in the electron density map and the structure is undoubtedly related with the charoite-90 polytype and in agreement with Merlino's OD model reported in the appendix of Rozhdestvenskaya *et al.* (2010).

TABLE 3. Bond lengths (Å) in charoite-96.

Na(1)−OH	2.35(7)	Na(2)−O(42)	2.29(5)	Ca(1)−(23)	2.23(4)	Ca(2)−O(25)	2.30(3)
−O(41)	2.36(5)	−O(45)	2.32(7)	−O(26)	2.33(2)	−O(38)	2.37(6)
−O(42)	2.43(4)	−O(41)	2.39(5)	−O(42)	2.33(4)	−O(23)	2.40(4)
−O(50)	2.48(3)	−O(49)	2.44(4)	−O(50)	2.38(4)	−O(50)	2.42(3)
−O(45)	2.49(7)	−OH	2.47(7)	−O(49)	2.43(4)	−O(49)	2.50(3)
−O(45)	2.64(7)	−OH	2.50(8)	−O(38)	2.44(6)	−O(41)	2.52(4)
Average	**2.46**		**2.40**		**2.36**		**2.41**
Ca(3)−O(9)	2.30(4)	Ca(4)−O(7)	2.24(4)	Ca(5)−O(6)	2.24(4)	Ca(6)−O(6)	2.36(4)
−O(18)	2.30(4)	−O(7)	2.25(4)	−O(18)	2.40(4)	−O(16)	2.36(4)
−O(4)	2.34(4)	−O(13)	2.27(4)	−O(20)	2.42(4)	−O(30)	2.37(4)
−O(9)	2.41(4)	−O(4)	2.40(4)	−O(8)	2.50(5)	−O(8)	2.40(5)
−O(13)	2.46(4)	−O(16)	2.42(4)	−O(35)	2.59(4)	−O(20)	2.42(4)
−O(7)	2.62(4)	−O(9)	2.42(5)	−O(33)	2.68(4)	−O(35)	2.46(4)
Average	**2.41**		**2.36**		**2.47**		**2.40**
Si(1)−O(4)	1.55(4)	Si(2)−O(6)	1.59(4)	Si(3)−O(8)	1.56(4)	Si(4)−O(13)	1.59(4)
−O(2)	1.59(4)	−O(7)	1.60(5)	−O(2)	1.59(5)	−O(11)	1.65(5)
−O(1)	1.63(3)	−O(5)	1.63(5)	−O(9)	1.64(5)	−O(10)	1.66(5)
−O(3)	1.65(4)	−O(3)	1.72(5)	−O(5)	1.66(5)	−O(12)	1.71(4)
Average	**1.61**		**1.63**		**1.61**		**1.65**
Si(5)−O(11)	1.57(4)	Si(6)−O(18)	1.55(3)	Si(7)−O(17)	1.55(5)	Si(8)−O(22)	1.59(4)
−O(14)	1.59(4)	−O(17)	1.64(3)	−O(14)	1.56(3)	−O(21)	1.64(4)
−O(16)	1.60(4)	−O(15)	1.67(4)	−O(20)	1.65(5)	−O(23)	1.67(4)
−O(15)	1.65(4)	−O(12)	1.67(4)	−O(19)	1.69(4)	−O(19)	1.73(3)
Average	**1.60**		**1.63**		**1.61**		**1.66**
Si(9)−O(25)	1.59(3)	Si(10)−O(26)	1.60(7)	Si(11)−(30)	1.50(4)	Si(12)−O(32)	1.55(4)
−O(22) × 2	1.63(4)	−O(21) × 2	1.59(3)	−O(27)	1.57(3)	−O(33)	1.61(3)
−O(24)	1.66(4)	−O(24)	1.61(5)	−O(28)	1.62(5)	−O(29)	1.62(5)
				−O(29)	1.73(4)	−O(31)	1.65(4)
Average	**1.63**		**1.60**		**1.61**		**1.61**
Si(13)−O(35)	1.59(4)	Si(14)−O(37)	1.58(5)	Si(15)−(39)	1.56(5)	Si(16)−(42)	1.51(7)
−O(34)	1.60(4)	−O(34)	1.62(4)	−O(41)	1.58(4)	−O(37)	1.58(4)
−O(28)	1.63(7)	−O(36)	1.65(5)	−O(36)	1.67(5)	−O(43)	1.63(4)
−O(32)	1.63(5)	−O(38)	1.68(5)	−O(40)	1.67(4)	−O(40)	1.66(4)
Average	**1.61**		**1.63**		**1.62**		**1.60**
Si(17)−O(39)	1.54(8)	Si(18)−O(46)	1.57(4)	Si(19)−(46)	1.62(7)	Si(20)−O(47)	1.60(3)
−O(44)	1.61(3)	−O(44) × 2	1.63(3)	−O(48)	1.62(6)	−O(48)	1.62(4)
−O(45)	1.63(7)	−O(47)	1.65(6)	−O(49) × 2	1.60(3)	−O(50) × 2	1.66(5)
−O(43)	1.65(5)						
Average	**1.61**		**1.62**		**1.61**		**1.64**

TABLE 3 (*contd*.).

Sr–O(33) × 2	2.45(5)	K(1)–O(3) × 2	2.77(4)	K(2)–O(1)	2.74(8)	K(4)–O(30) × 2	2.66(5)
–O(8) × 2	2.95(6)	–O(10)	2.85(10)	–O(11) × 2	2.80(4)	–O(33) × 2	2.66(6)
–O(30) × 2	3.07(5)	–O(5) × 2	2.87(6)	–O(12) × 2	2.83(5)	–O(6) × 2	3.15(4)
		–O(2) × 2	3.17(4)	–O(15) × 2	2.86(4)		
		–O(13) × 2	3.35(4)	$-H_2O$	3.22(8)		
				–O(4) × 2	3.30(4)		
Average	**2.82**		**3.02**		**2.95**		**2.82**
K(3)–O(21)	2.79(4)	K(5)–O(22) × 2	2.90(5)	K(6)–O(36)	2.81(6)	H_2O–O(24)	2.56(9)
–O(15)	2.81(4)	–O(21) × 2	3.31(5)	–O(29)	2.84(7)	–O(15) × 2	2.80(5)
–O(14)	2.83(3)	–O(17) × 2	3.31(6)	–O(40)	2.87(6)	–K(3) × 2	2.87(4)
$-H_2O$	2.87(4)	–O(14) × 2	3.34(3)	–O(28)	3.08(6)	–K(2) × 2	3.22(8)
–O(24)	2.87(4)			–O(19)	3.13(5)		
–O(22)	2.89(4)			–O(37)	3.15(6)		
–O(34)	2.90(4)			–O(32)	3.19(8)		
–O(17)	2.96(5)						
–O(38)	3.20(7)						
–O(35)	3.21(4)						
Average	**2.93**		**3.21**		**3.01**		

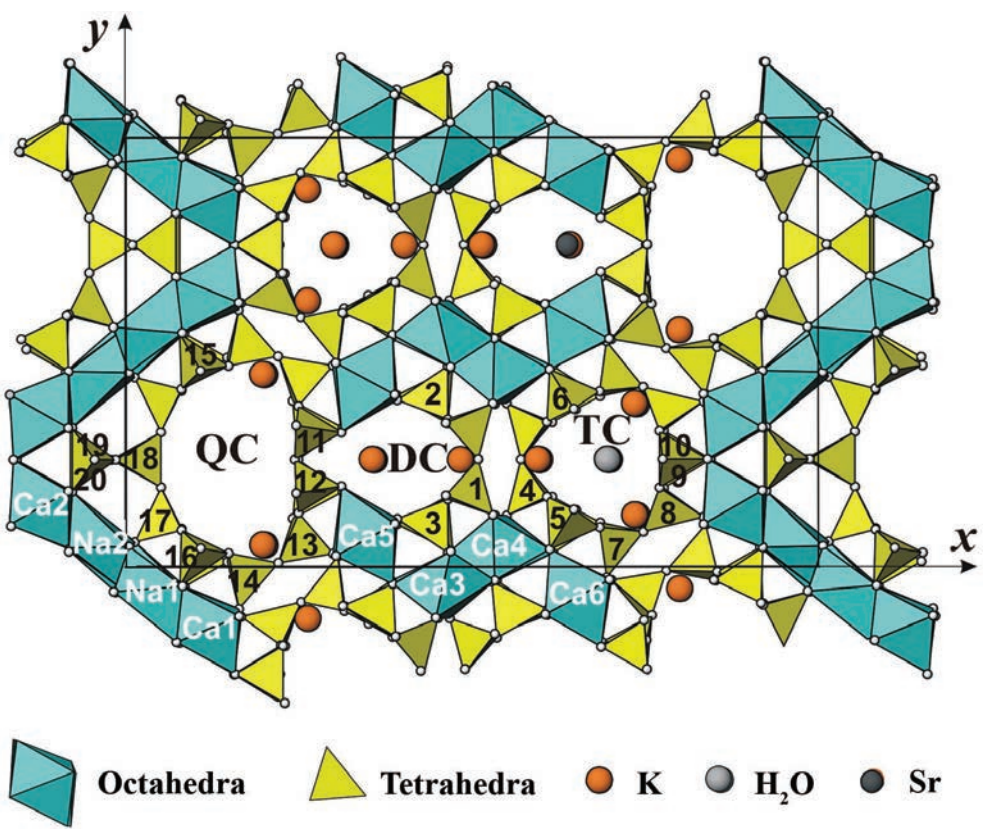

FIG. 5. The crystal structure of charoite-96 in projection along [001]: **QC** refers to the tubular hybrid *dreier* quadruple chain; **DC** refers to *dreier* double chain; **TC** refers to the tubular loop-branched *dreier* triple chain. The numbers correspond to atom sites listed in Table 2.

Results and discussion

Structure overview

In a projection along [001] (Fig. 5) the structure of charoite-96 is similar to the structure of charoite-90, which was described in detail by Rozhdestvenskaya *et al*. (2010). Both polytypes are composed of three different silicate chains parallel to the *z* axis: a *dreier* double chain, $[Si_6O_{17}]^{10-}$, a tubular loop-branched *dreier* triple chain, $[Si_{12}O_{30}]^{12-}$ and a tubular hybrid *dreier* quadruple chain, $[Si_{17}O_{43}]^{18-}$, these are described as the **DC**, **TC** and **QC**, respectively. The chains share their apical oxygens with bands of (Ca,Na)-octahedra, which vary in width. The K^+ and Sr^{2+} cations and H_2O molecules are located inside the channels formed by the silicate chains.

Octahedral columns

Edge-sharing alternating Na(1)–Na(2), Ca(1)–Ca(2), Ca(3)–Ca(4), Ca(5)–Ca(6) octahedra extend parallel to the *z* axis (Figs 5 and 6). Bands, four octahedra wide, are created by columns of Ca(1)–Ca(2) octahedra sharing edges with columns of Na(1)–Na(2) octahedra. Apical oxygens link two such bands to form a continuous zigzag sheet parallel to (100). Columns of Ca(5)–Ca(6) octahedra are linked via apical oxygens to columns of Ca(3)–Ca(4) octahedra and form isolated bands four octahedra wide. The *c* lattice parameter is ~7.2 Å and spans two octahedral edges. In principle this permits the silicate chains connect to the octahedral fragment at two distinct positions ~3.6 Å apart. The octahedral *M*–O bond distances vary from 2.36

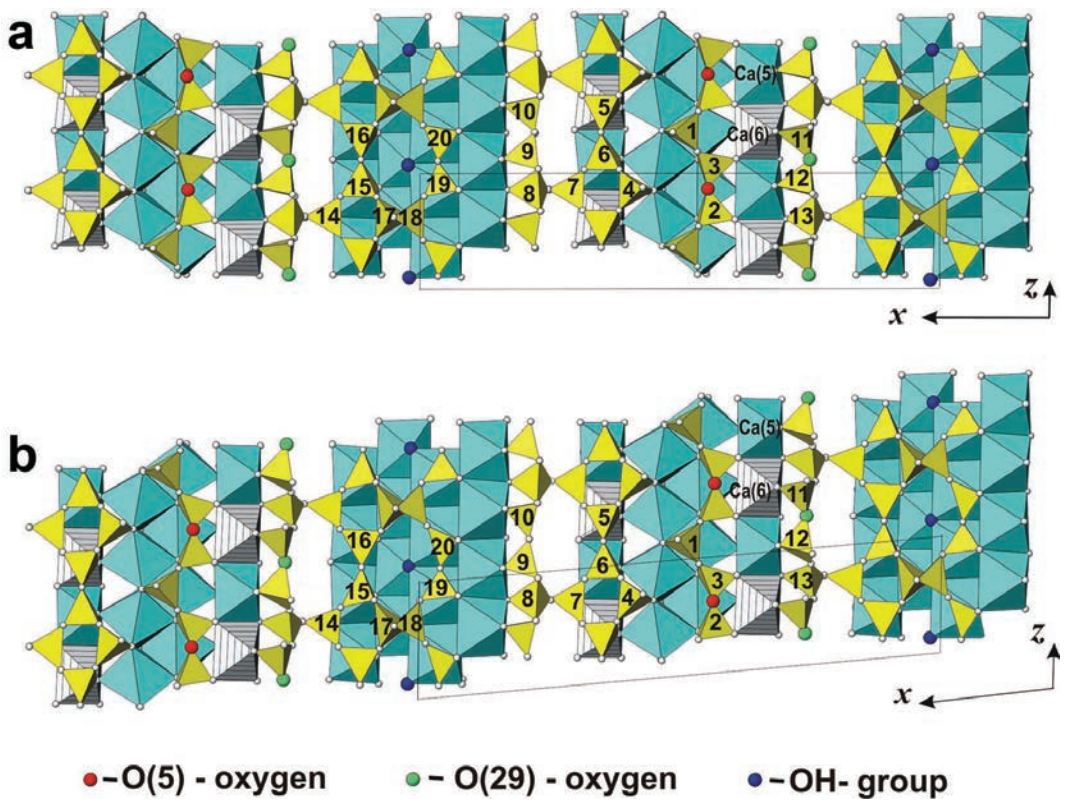

FIG. 6. Bounded projection of (*a*) charoite-90 and (*b*) charoite-96 polytypes ($0.32 < y < -0.25$) in [010] projection. For the sake of simplicity, only the front side of the silicate chains is shown. The large blue circles mark OH^- groups. The large red and green circles mark the O5 and O29 sites in **DC** and **QC**, respectively. Note that in comparison to charoite-90, in charoite-96 the chains on either side of the octahedral column containing (Ca(5)–Ca(6)) are shifted by $z = ½$ with respect to one another. The numbers correspond to atom sites listed in Table 2.

to 2.47 Å (Table 3). In common with charoite-90, most of the octahedrally-coordinated sites in charoite-96 are occupied by Ca, but two sites, Na(1) and Na(2), contain Na predominantly (Table 2). One of the two anion positions shared by the Na-octahedra is occupied by OH^- (or F^-).

Silicate chains

The **DC** is the same type as the chain in xonotlite (Kudoh and Takeuchi, 1979; Hejny and Armbruster, 2001); it consists of two *dreier* single chains [tetrahedra Si(1)–Si(3)] (Figs. 5 and 6). The tubular **TC** consists of three loop-branched *dreier* single chains [two chains of tetrahedra Si(4)–Si(7) and one chain of tetrahedra Si(8)–Si(10)] and has approximately three-fold local symmetry. Similar loop-branched *dreier* single chains are also present in synthetic $Li_2Mg_2[Si_4O_{11}]$ (Czank and Bissert, 1993). The tubular **QC** consists of a *dreier* double chain [tetrahedra Si(11)–Si(13)], two loop-branched *dreier* single chains [tetrahedra Si(14)–Si(17)], and a *dreier* single chain [tetrahedra Si(18)–Si(20)]. The *dreier* single chain is similar to that found in wollastonite and the *dreier* double chain is of the type found in okenite (Merlino, 1983).

The three different chains lie on mirror planes at y = ¼ and ¾ and alternate along the x axis (Figs 5 and 7). The **TC** is surrounded by one **DC** and two **QC** in such a way that each of the three horizontal Si_2O_7 groups of the **TC** has a horizontal Si_2O_7 group of one of the surrounding chains as a neighbour. Neighbouring Si_2O_7 groups connect octahedra in such a way that they are shifted along c by one octahedral edge with respect to each other (Fig. 7).

One of the single chains of the **DC** [tetrahedra Si(1)–Si(3)] and one of the chains of the **TC** [tetrahedra Si(4)–Si(7)] join with the same band of octahedra Ca(3)–Ca(6), whereas the other symmetrically equivalent parts of the **DC** and **TC** join to another band of octahedra [Ca(3)–Ca(6)] (Figs 5 and 6). The chain of tetrahedra Si(8)–Si(10) of the **TC** is joined with two columns of Ca(1)–Ca(2) octahedra.

The chain of tetrahedra Si(11)–Si(13) in the **QC** is connected to columns of Ca(5)–Ca(6) octahedra. The chains of tetrahedra Si(14)–Si(17) and of tetrahedra Si(19), Si(20) join with bands of Na(1)–Na(2)–Ca(1)–Ca(2) octahedra. The Si(18)

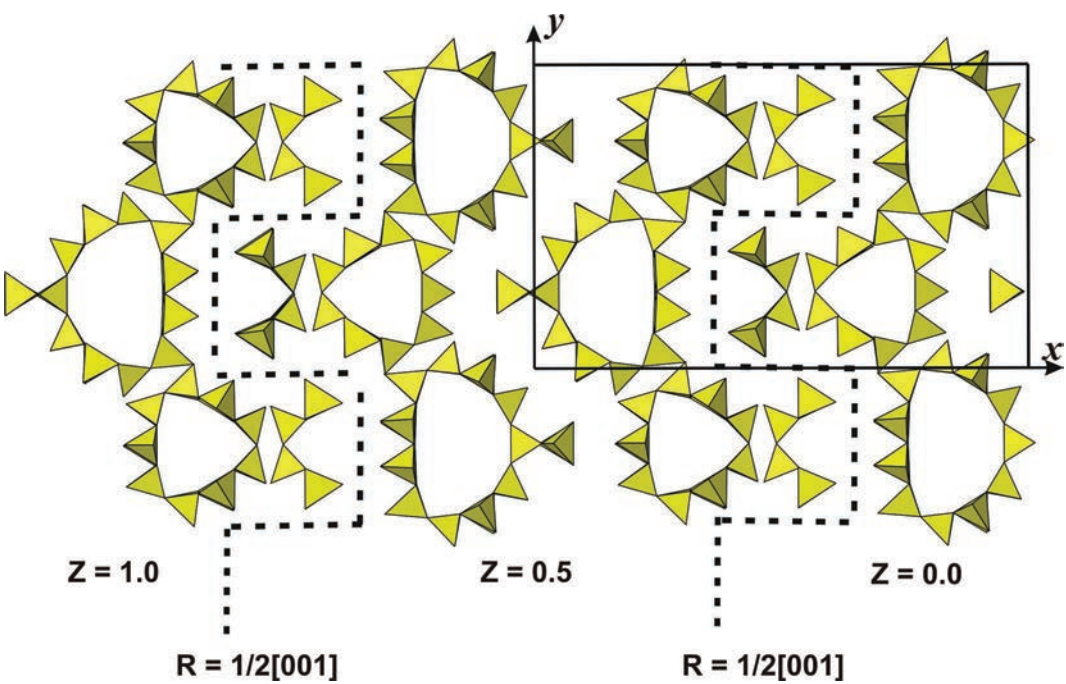

FIG. 7. The dashed line indicates the shift or 'stacking fault' plane. In charoite-96 every unit cell is shifted by z = ½.

tetrahedron is unique as it connects to four surrounding tetrahedra and therefore has the same connectivity as silicate tetrahedra in tectosilicate minerals. A comparison of the unit-cell parameters of charoite-90 [a = 31.96(6), b = 19.64(4), c = 7.09(1) Å, β = 90.0(1)º] and charoite-96 [a = 32.11(6), b = 19.77(4), c = 7.23(1) Å, β = 95.85(9)º] shows that the main difference between them is in the value of the angle β.

The angle β of 96º in the charoite-96 unit cell is produced by a shift by $-c/2$ in comparison to the unit cell of charoite-90. Due to the spatial relationship between the octahedral bands and *dreier* chains this means that in charoite-96 the tetrahedral chains are shifted by $c/2$ along the octahedral bands in each subsequent unit cell. This is in keeping with OD features; the unit cells of both charoite-96 and charoite-90 contain two OD layers, but in charoite-96 two applications of the σ-operation $2_{-1/2}$ produce a shift of $c/2$ and a β angle of 96º, whereas in charoite-90, the alternation of the $2_{1/2}$ and $2_{-1/2}$ operations, produce zero shift and a β angle of 90º.

As there are three different tetrahedral chains, it is useful to determine where the shifts take place. For a convenient comparison of both polytypes the coordinates of the atoms in charoite-90 given in Rozhdestvenskaya *et al*. (2010) have been transformed by the matrix (−1 0 0 / 0 −1 0 / 0 0 1). In Fig. 6*a*,*b* bounded projections ($-0.25 < y < 0.32$) of the structures of charoite-90 and charoite-96 polytypes are shown. Although each of the **DC**, **TC** and **QC** is composed of different *dreier* single chains and/or loop-branched *dreier* single chains which could, in principle, fit separately to the sub-periodicity of the octahedral columns, it can be supposed that they form a module that is shifted as a rigid block. This is forced by the arrangement of the horizontal Si_2O_7 groups of neighbouring chains.

All corners of the octahedra are connected with apices of the silicate tetrahedra by shared oxygens with one exception. This is the corner between three Na octahedra which is occupied by an OH^- group (or by F^-). In a view perpendicular to the octahedral band the OH^- group seems to be positioned at the centre of an 8-membered ring of the **QC** (compare the dark-blue circles in Fig. 6). As the OH^- group cannot serve as a link to a silicate tetrahedron, this situation does not permit a shift of the **QC** along the octahedral motif and thus fixes the position of this **QC** in the structure. The OH^- group across the centre of symmetry on the other side of the zigzag wall plays the same role and fixes the **QC** on the other side of the zigzag wall. In other words, by virtue of an exclusion condition, the octahedral edge $OH^- - OH^-$ plays the role of a pin and fixes the mutual position of two **QC**s and thus does not permit a shift of these chains along the octahedral wall.

Horizontal Si_2O_7 groups of each of the chains in the **DC**, **TC** and **QC** connect separate bands of Ca octahedra in such a way that the apical oxygens of neighbouring Si_2O_7 groups are joined alternately to the corners on edges of octahedra parallel to the z axis and therefore, adjacent chains are shifted relative to each other by half a translation along the z axis (Fig. 6). Thus, their mutual positions are fixed and it is evident that all three chains, **DC**, **TC** and **QC**, should be shifted jointly.

Taking into account the constraints described above one can see that the mutual location of **QC** [tetrahedra Si(11)−Si(20)] and **TC** [tetrahedra Si(4)−Si(10)] is the same as in charoite-90 (Fig. 6*a*,*b*). Their mutual location is determined by Si(7)−Si(8) and Si(13)−Si(14) tetrahedra, which are joined with edges of columns of Ca(1)−Ca(2) and Ca(5)−Ca(6) octahedra parallel to the z axis. The mutual location of **TC** and **DC** [Si(1)−Si(3)] is also the same as in charoite-90. This is determined by tetrahedra Si(1) and Si(4), which are joined with edges of columns of Ca(3)−Ca(4) octahedra parallel to the z axis.

A different situation is observed for the mutual location of the **DC** [tetrahedra Si(1)−Si(3)] and the **QC** [tetrahedra Si(11)−Si(20)]. In Fig. 6*a*,*b* the large red and green circles mark the oxygen O5 and O29 sites, shared between Si_2O_7 groups parallel to the z axis [Si(2)−Si(3)] in the *dreier* single chain of **DC** and [Si(11)−Si(12)] in the *dreier* single chain of **QC**, respectively. In this section of the charoite-96 structure the *dreier* single chain [Si(11)−Si(13)] is shifted by $c/2$ with respect to the chain [Si(1)−Si(3)]. As **DC**, **TC** and **QC** have to be shifted simultaneously, the shift of the modules takes place on the isolated octahedral bands Ca(3)−Ca(6). In Fig. 7 the border of the shifts, which may be compared with the border between OD layers in Fig. 1, is shown schematically. This can be described as an undulating plane parallel to (100) with a shift vector of ½[001]. The surface is not planar in the proper sense, but following Veblen (1985) one can say that these shifts describe complex surfaces which "can be lumped with truly planar defects for simplicity".

Conclusions

Automated diffraction tomography is a useful method for studying the crystal structures of polyphasic nanocrystalline materials including intergrowths of fibrous silicates such as charoite-90 and charoite-96. Charoite-96 and charoite-90 are polytypic and correspond to the two MDO structures in the charoite OD family. Relatively rigid building blocks, or modules, made up of pairs of OD layers, are present in both polytypes. The structural reasons for the internal rigidity of the modules and the ambiguity in the linker position between the modules are identified. Stacking along the x direction of the modules without shifts (Fig. 8*a*) results in charoite-90, whereas periodic shifts of $c/2$ (Fig. 8*b*) result in charoite-96. A structure with alternating shifts of $+c/2$ and $-c/2$ (Fig. 8*c*) produces an ordered polytype with a doubled a lattice parameter, whereas random shifts produce a polytype with disorder along the x axis. Both of these polytypes have been identified (Fig. 2*c*,*d*) and named charoite-2a and charoite-d, respectively. More complex regular sequences of + and − shifts are able to produce polytypes with lattice parameters $a' = n{\cdot}a$ (n = 3, 4, 5...), in a similar manner to wollastonite. To date, coherently scattering samples of charoite-2a in nanoscale fibres of charoite that are large enough for ADT acquisition have not been identified. Nevertheless, in the light of the results on charoite-90 and charoite-96 and considering the almost perfect agreement between theory and experiment, we believe that painstaking searches for pure charoite-2a and other possible polytypes are not as pressing as they were before the structures of charoite-90 and charoite-96 were known.

It is noteworthy that adoption of a structural model based on similar crystal chemical systems (Czank and Liebau, 1980; Rozhdestvenskaya and Nikishova, 2002) and the application of symmetry-oriented OD-theory (Dornberger-Schiff, 1956, 1964, 1966; Merlino, 1997) produced a prediction of polytypism in charoite which is corroborated by the *ab initio* structure solution of charoite-96 performed by ADT. After more than 50 years of attempts to determine the enigmatic nature of the charoite structure (Chiragov and Shirinova, 2004; Nikishova *et al*., 1985; Rozhdestvenskaya *et al*., 2009) the problem has been solved.

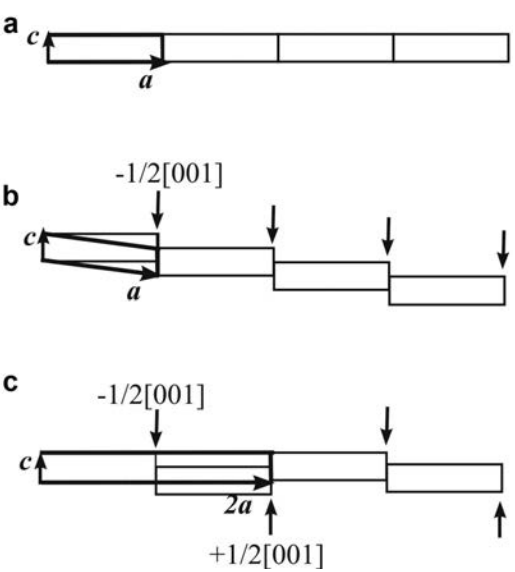

FIG. 8. Schematic drawing of the charoite polytypes: (*a*) charoite-90; (*b*) charoite-96; (*c*) charoite-2a. Arrows indicate the shift vectors characteristic of the specific polytype.

Acknowledgement

The authors thank the Deutsche Forschungsgemeinschaft for financial support (DE 412/44-1, SP1415 and SFB 625).

References

Akselrud, L.G., Grin, Yu.N., Zavalii, P.Yu., Pecharsky, V.K. and Fundamensky, V.S. (1989) CSD − the programs for determination and refinement of crystal structures. *Collected Abstracts of the XII European Crystallography Meeting*, *Moscow*, **3**, 155.

Bailey, S.W. (1977) Report of the I.M.A. − I.U.Cr. Joint Committee on Nomenclature. *American Mineralogist*, **62**, 411−415.

Burla, M.C., Caliandro, R., Camalli, M., Carrozzini, B., Cascarano, G.L., De Caro, L., Giacovazzo, C., Polidori, G., Diligi, S. and Spagna, R. (2007) *IL MILIONE*: a suite of computer programs for crystal structure solution of proteins. *Journal of Applied Crystallography*, **40**, 609−613.

Chiragov, M.I. and Shirinova, A.F. (2004) Crystal structure of charoite; relations to structures of miserite, canasite and okenite. *Mineralogicheskiy Zhurnal*, **26**, 5−9, [in Russian].

Czank, M. and Bissert, G. (1993) The crystal structure of $Li_2Mg_2[Si_4O_{11}]$, a loop-branched dreier single chain silicate. *Zeitschrift für Kristallographie*, **204**, 129−142.

Czank, M. and Liebau, F. (1980) Periodicity faults in chain silicates: a new type of planar lattice fault observed with high resolution electron microscopy. *Physics and Chemistry of Minerals*, **6**, 85–93.

Dornberger-Schiff, K. (1956) On order–disorder structures (OD-structures). *Acta Crystallographica*, **9**, 593–601.

Dornberger-Schiff, K. (1964) Grundzüge einer Theorie der OD-Strukturen aus Schichten. *Abhandlungen der Deutschen Akademie der Wissenschaften zu Berlin, Klasse für Chemie, Geologie und Biologie*, **3**, 1–107.

Dornberger-Schiff, K. (1966) *Lehrgang über OD Strukturen*. Akademie Verlag, Berlin, 135 pp.

Ferraris, G., Makovicky, E. and Merlino, S. (2004) *Crystallography of Modular Materials*. Oxford University Press, Oxford, UK, 370 pp.

Hejny, C. and Armbruster, T. (2001) Polytypism in xonotlite $Ca_6Si_6O_{17}(OH)_2$. *Zeitschrift für Kristallographie*, **216**, 396–408.

Jefferson, D.A. and Bown, M.G. (1973) Polytypism and stacking disorder in wollastonite. *Nature Physical Science*, **245**, 43–44.

Kolb, U., Gorelik, T., Kübel, C., Otten, M.T. and Hubert, D. (2007) Towards automated diffraction tomography: part I – data acquisition. *Ultramicroscopy*, **107**, 507–513.

Kolb, U., Gorelik, T. and Otten, M.T. (2008) Towards automated diffraction tomography. Part II – cell parameter determination. *Ultramicroscopy*, **108**, 763–772.

Kudoh, Y. and Takeuchi, Y. (1979) Polytypism of xonotlite: (I) structure of an A1 polytype. *Mineralogical Journal*, **9**, 349–373.

Liebau, F. (1985) *Structural Chemistry of Silicates*. Springer-Verlag, Berlin, 412 pp.

Merlino, S. (1983) Okenite, $Ca_{10}Si_{18}O_{46}{\cdot}18(H_2O)$; the first example of a chain and sheet silicate. *American Mineralogist*, **68**, 614–622.

Merlino, S. (1997) OD approach in minerals: examples and applications. Pp. 29–54 in: *Modular Aspects of Minerals* (S. Merlino, editor). EMU Notes in Mineralogy **1**, Eötvös University Press, Budapest, 488 pp.

Mugnaioli, E., Gorelik, T. and Kolb, U. (2009) "Ab initio" structure solution from electron diffraction data obtained by a combination of automated diffraction tomography and precession technique. *Ultramicroscopy*, **109**, 758.

Mugnaioli, E., Gorelik, T., Stewart, A. and Kolb, U. (2011) "Ab-initio" structure solution of nanocrystalline minerals and synthetic materials by automated electron tomography. In: *Minerals as Advanced Materials II* (S.V. Krivovichev, editor). Springer-Verlag, Berlin, 427 pp.

Nikishova, L.V., Lazebnik, K.A. and Lazebnik, Yu.D. (1985) About crystallochemical formulae of charoite. Pp. 100–105 in: *Crystal Chemistry and Structure of Minerals*. Nauka, Leningrad, Russia, [in Russian].

Rozhdestvenskaya, I.V. and Nikishova, L.V. (2002) Crystallochemical characteristics of alkali calcium silicates from charoitites. *Crystallography Reports*, **47**, 545–554.

Rozhdestvenskaya, I.V., Kogure, T. and Drits, V.A. (2009) Structural model of charoite. *Mineralogical Magazine*, **73**, 883–890.

Rozhdestvenskaya, I.[V.], Mugnaioli, E., Czank, M., Depmeier, W., Kolb, U., Reinholdt, A. and Weirich, T. (2010) The structure of charoite, $(K,Sr,Ba,Mn)_{15-16}(Ca,Na)_{32}[(Si_{70}(O,OH)_{180})](OH,F)_{4.0}{\cdot}nH_2O$, solved by conventional and automated electron diffraction. *Mineralogical Magazine*, **74**, 159–177.

Sheldrick, G.M. (2008) A short history of *SHELX*. *Acta Crystallographica*, **A64**, 112–122.

Schömer, R., Heil, U., Schlitt, S. and Kolb, U. (2009) *ADT-3D. A software package for ADT data visualizing and processing*. Institute of Computer Science, Johannes Gutenberg University, Mainz, Germany.

Veblen, D.R. (1985) Direct TEM imaging of complex structures and defects in silicates. *Annual Review of Earth and Planetary Sciences*, **13**, 119–146.

Vincent, R. and Midgley, P.A. (1994) Double conical beam-rocking system for measurement of integrated electron diffraction intensities. *Ultramicroscopy*, **53**, 271–282.

Wenk, H.R., Muller, W.F., Liddell, N.A. and Phakey, P.P. (1976) Polytypism in wollastonite. Pp. 324–331 in: *Electron Microscopy in Mineralogy* (H.R. Wenk, editor). Springer-Verlag, Berlin, 564 pp.